Original Research

Single Step Green Method of Synthesis for Activated Carbon from Lignocellulosic Biomass Waste of *Jacaranda mimosifolia* for Sustainable Water Purification

Vishal Haribhai Patel [1,2], Dr. Abdul Gani[3, †], Dr. Anamika Paul[4]

[1]*School of Engineering, Galgotias University. Plot No.2, Sector 17-A, Yamuna Expressway, Greater Noida, Uttar Pradesh, India, Pin- 201310*, ORCID ID: 0000-0001-9217-3029 Email: vishalhpatel2003@yahoo.co.in

[2]*Amity University Uttar Pradesh, Room No. G05, J3 Block, Amity University Uttar Pradesh, Noida, Pin – 201313* Email: vpatel@amity.edu

[3]*School of Engineering, Galgotias University. Plot No.2, Sector 17-A, Yamuna Expressway, Greater Noida, Uttar Pradesh, India, Pin- 201310* ORCID ID: 0000-0001-5525-6642 E-mail: abdul.gani@galgotiasuniversity.edu.in

[4]*WSP Global Inc. 1st Floor, FC24, Sector 16A, Noida, Uttar Pradesh Pin- 201306* ORCID ID: 0000-0001-9932-2867 Email: anamika.paul@wsp.com

† Corresponding author: E-mail: abdul.gani@galgotiasuniversity.edu.in

Abstract

Abundant lignocellulosic biomass components have been a source of inspiration for designing complex materials with high surface area and potent applications in wide variety of commercial products including water purification, biosensors, catalysis and others. Billion tons of lignocellulosic biomass waste are produced in a year. These lignocellulosic biomass waste could be the good source of precursor for activated carbon and other carbon-based nanomaterials. Activated carbon were prepared from Seed pods of lignocellulosic biomass of *Jacaranda mimosifolia* which treated as waste using single step green method of synthesis. Synthesized activated carbon was characterized using high resolution scanning electron microscopy (HRSEM), X-ray diffraction (XRD), Fourier transform infrared spectroscopy (FTIR), N_2 adsorption/desorption and Zeta potential. It was evident that the synthesis method was free from chemical use and thus eco-friendly. We have reported maximum removal of heavy metal, lead ion (Pb^{+2}) and dye Eriochrome Black T (EBT) using prepared activated carbon was 58.77 and 286.56 mg·g^{-1} respectively. The adsorption was rapid with 97% of Pb^{+2} and 90% of EBT adsorption accomplished within 60 min. The synthesized material could be used in design of filter for sustainable water purification.

1. Introduction

Many organic and inorganic water-soluble pollutants are discharging into waters bodies give rise to serious environmental problems. The wastewater, produced from various industries such as manufacturing, printing, textile(Yao et al. 2020), chemicals, electronics, and pharmaceutical industries(Özdemir et al. 2019) carry a noticeable quantity of pollutants including dyes and heavy metals this has remained major environmental

challenge. They are responsible for the seepage of different pollutants such as dyes(Tonato et al. 2019), heavy metals, phenols(Mohammed et al. 2018), into the aquatic environment without proper removal. Both heavy metals and dyes are envisaged to be some of the most dangerous pollutants in water systems as they exhibit mutagenic, immunogenic, carcinogenic, and teratogenic characteristics(Azari et al. 2019) also causes serious environmental and health problems for aquatic flora, fauna, and finally human health(Yin et al. 2019).

Dyes are used in a varied sectors including textile, paper, leather, dyestuff, printing, plastic, cosmetics, and coatings because of low-cost, brightness, and high resistance against environmental conditions(Reck et al. 2018). Moreover, dyes are very stable to light, temperature and microbial attack and even at low concentrations, they are optically active and detectable(Bello et al. 2018) causing very acute impact on water bodies(dos Santos et al. 2018).

Industries generating a massive quantity of heavy metals laden wastewater contains arsenic, cadmium, lead, cobalt, copper, chromium, mercury, zinc, iron, manganese, nickel, and others. These effluents are released into water bodies without proper treatment(Liu et al. 2019)(Dobrowolski et al. 2019) and poisonous at low concentrations(Ali et al. 2019), can be bio-accumulated/magnified along with food chains and pose hazards to human health(Que et al. 2019) and found within the different environmental compartments(Alonso-Magdalena et al. 2019). Owing to the mentioned impacts on different biota, a strong demand for water purification from heavy metals and dyes becomes crucial.

The key techniques that are used to remove pollutants from the water phase includes physical and chemical processes include coagulation/flocculation(Hou et al. 2019), precipitation(Chen et al. 2018), ultrafiltration(Kavitha et al. 2019), photo-oxidation(Du & Chen 2018), electrodialysis(Nemati et al. 2017), electrocoagulation(Doggaz et al. 2019), membrane separation(Hosseini et al. 2018), ion exchange(Feng et al. 2019), forward osmosis(Qiu & He 2019), electrochemical oxidation of Wastewater(Rai & Sinha 2022), irradiation(Ghobashy & Elhady 2017), and adsorption(Wei et al. 2021). Whilst the biological processes include phytoextraction(Napoli et al. 2019) and biological degradation(Jacob et al. 2018).

In the past few years, bio templates from natural sources like extracts of various plant components have been a source of inspiration for designing complex materials with high surface area which have potent applications in wide variety of commercial products including filters for water purification, biosensors, catalysis and others.

Biosorption, using of bio-wastes for the elimination of different water pollutants is an eco-friendly, economic, and efficient technique(Gupta et al. 2018) which limit the concentration of different water pollutants to the acceptable limits recommended by different federal regulations(Krstić et al. 2018). Numerous benefits are attained due to recycling of these biomasses including waste minimization and can rectify different ecological as well as environmental problems(Gupta et al. 2019). Adsorption using a low-cost and sustainable biosorbent derived from biomass provides alternative towards a circular economy(Madeła & Skuza 2021).

Jacaranda mimosifolia used in the study belongs to the botanical family Bignoniaceae, is reported to be native to South America. The jacaranda has been cultivated in almost every part of the world and used in numerous metropolises in tropical and sub-tropical countries as ornamental tree(M Mostafa et al. 2014)(Ragsac et al. 2019). *Jacaranda mimosifolia* can be categorized as a medium-sized tree which is usually less than 10 m tall and can reach 12-15 m under ideal conditions(*Agroforestree database*). Seed pods, drying dark brown, have compressed-elliptical shape and are 3.5–8.5 cm long. Seeds surrounded by a thin membrane usually 0.8–1.4 cm long. Its seed pods are not edible and are also not attractive to birds as they do not have a pleasant aroma and colour, therefore upon ripening, they dry and fall, generating a large amount of organic biomass over the soil. Very limited studies in the literature have been found related to the use of *Jacaranda mimosifolia* seed pods (JMSP) for the removal of heavy metal pollutants from water or wastewater.

In present study, activated carbons (biosorbent) for water treatment have been synthesized using biomass of JMSP to investigate the adsorption performance on Pb^{+2} and Eriochrome Black T (EBT) in aqueous solution. The effect of various operational parameters, kinetics, thermodynamics, adsorption isotherms were investigated and investigate the adsorption mechanism by combining different methods including high resolution scanning electron microscopy (HRSEM), X-ray diffraction (XRD), Fourier transform infrared spectroscopy (FTIR), N_2 adsorption/desorption and Zeta potential.
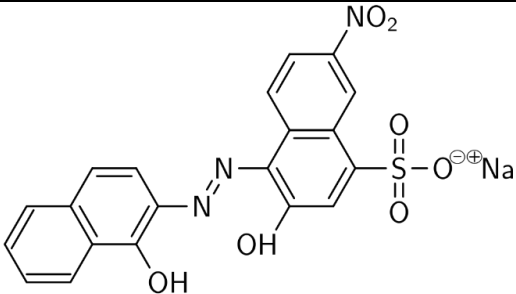
2. Materials and methods

2.1 Chemicals and Reagents used

The JMSP were collected from local city gardens of greater noida, India. Reagents used in experiments were analytical grade and no furthered processing was carried out before using. Unless specify, the deionized water (18.2 MΩ·cm) was used during all experiment. The standard stock solutions of 1000 mg·L^{-1} were prepared for

metal ion Pb^{+2} and EBT, table 1 describe the specification and chemical structure of EBT used for study. The pH of the solution was adjusted using 0.01-1 M HCl and NaOH.

Table 1. Specification and Chemical Structure of Eriochrome Black T (EBT)

Dye Name	IUPAC Name	Chemical Formula & Molecular Weight	Chemical Structure	λ_{max} (nm)
Eriochrome Black T (EBT)	sodium;4-[(1-hydroxynaphthalen-2-yl) hydrazinylidene]-7-nitro-3-oxonaphthalene-1-sulfonate CAS Number 1787-61-7	$C_{20}H_{12}N_3O_7SNa$ 461.381 g·mol^{-1}		526

2.2 Preparation of activated carbon

The seeds were removed from the collected JMSP before processing them. First, collected JMSP were washed with tap water to remove the residual dirt, sand and other soluble impurities, than washed with deionized water 4 times. Washed JMSP were dried in laboratory oven at 70 ^{0}C for 24 h until constant weight. The dried JMSP was ground using electronic blender and sieved into the particles < 177 μm and stored into the plastic bottles. The sieved JMSP powder was placed into the specially designed reactor under the inert atmosphere with N_2 flow rate of 0.001 m^3·min^{-1} with heating rate maintained at 300 ^{0}C·min^{-1} to the final temperature of 1950 ^{0}C, which was maintained for 05 minutes (carbonization) followed by activation at 1950 ^{0}C under CO_2 with flow rate of 0.001 m^3·min^{-1} for 05 minutes. The temperature of 1950 ^{0}C was maintained for total time of 10 minutes, 05 minutes for carbonization and 05 minutes for activation. The prepared activated carbon left for cooling to room temperature and washed with deionized water; the activated carbon was separated using 0.45 μm nylon membrane filter. The activated carbon obtained was dried at 110 ^{0}C for 24 h, cooled to room temperature in desiccator and kept in airtight bottles for further analysis. The prepared activated carbon was labelled as JMSP AC. The single step synthesis method for production of activated carbon (biosorbent) is efficient and free from use of chemical and/ chemical treatment thus eco-friendly. Further, the synthesis method is scalable and has flexibility in its operation. The quantitative analysis (table 2) confirms the higher conversion of available elemental carbon from lignocellulosic biomass to the activated carbon using the proposed synthesis method.

Table 2. Proximate analysis of synthesized JMSP activated carbon.

Particular	Moisture % on dry basis	Volatile matter % on dry basis	Ash % on dry basis	Fixed carbon % on dry basis
JMSP AC	6.67	22.26	3.03	74.71

The percent yield of JMSP AC was determined from the relation:

$$Yield(\%) = \frac{w_{ac}}{w_0} x\ 100 \tag{1}$$

where w_{ac} and w_0 were final JMSP AC dry weight(g) and the precursor dry weight (g), respectively.

2.3 Adsorption studies

Efficacy of the synthesized JMSP AC was tested as adsorbent for the Pb^{+2} and EBT sorption from aqueous solutions in the batch experiments. All experiments were triplicate and mean of these were reported with control experiment in the same operating conditions without adding adsorbent. Different standard solutions (10ppm, 25 ppm, 50 ppm, 75 ppm, 100 ppm, 125 ppm, 150 ppm) of Pb^{+2} metal ion and (10 ppm, 25 ppm, 50 ppm, 100 ppm, 200 ppm, 300 ppm, 400 ppm, 500 ppm) for EBT dye were prepared and kept in refrigerator to maintain the constant volume and concentration. The adsorption experiments were carried out in 250 ml flask containing 100 ml of metal and dye solution of various concentration, dosage of JMSP AC and contact time at natural solution pH. Samples were

shaken in thermostat incubator at 200 rpm for 2 h. The residual metal ion concentration was determined using ICP-OES (Agilent technologies 700 series) and that of dye was determined using UV-VIS spectrophotometer (Agilent Carry 100 UV-Vis). The amount of metal ion and dye adsorbed per unit mass of adsorbent was calculated according to equation:

$$Q_e = \frac{(C_0 - C_e)V}{W} \tag{2}$$

where the quantity Q_e is the amount of metal ion/dye adsorbed on biosorbent (mg·g^{-1}), C_0 and C_e are the initial and equilibrium concentration of metal ion/dye solution (mg·L^{-1}). V is the volume of metal ion/dye solution (L) and W is the amount of JMSP AC biosorbent (g).

The % removal was determined by following equation:

$$\text{Removal (\%)} = \frac{(C_0 - C_e)}{C_0} \ x \ 100 \tag{3}$$

The adsorption kinetics were done at 25 ^{0}C and natural pH with concentration at 100 and 250 mg·L^{-1} for metal ion and dye respectively. The samples were analyzed at predefined time intervals and metal ion/dye uptake on biosorbent at time t was determined using Eq. 4

$$Q_t = \frac{(C_0 - C_t)V}{W} \tag{4}$$

where C_t (mg·L^{-1}) is concentration of metal ion/dye at any time.

The adsorption isotherm data were analysed using four different types of adsorption isotherm models including the Langmuir, Freundlich, Temkin and Redlich-Peterson (R-P); the kinetic models used were pseudo-first-order, pseudo-second order and intraparticle diffusion (table 3).

Table 3. Adsorption isotherms and kinetic models.

Models	Equation	Parameters
Langmuir	$Q_e = \frac{Q_m K_L C_e}{1 + K_L C_e}$	K_L = constant related to the affinity of binding sites (L·mg^{-1})
Freundlich	$Q_e = K_F C_e^{1/n}$	K_F = constant related to adsorption capacity (L·g^{-1}), n = constant related to intensity of adsorption
Temkin	$Q_e = \frac{RT}{B_T} ln(A_T C_e)$	A_T = equilibrium binding constant (L·g^{-1}), R = universal gas constant (8.314 J·mol^{-1} K^{-1}), T = absolute temperature (K), B_T = constant related to adsorption heat (J·mol^{-1})
Redlich-Peterson (R-P)	$Q_e = \frac{K_R C_e}{1 + a_R C_e^{\ g}}$	K_R = R-P constant (L·g^{-1}) a_R = R-P constants (L·mg^{-1}) g = exponent related to surface heterogeneity
Pseudo-first order	$Q_t = Q_e(1 - e^{-k_1 t})$	k_1 = equilibrium rate constant (min^{-1})
Pseudo-second order	$Q_t = \frac{Q_e^2 k_2 t}{1 + Q_e k_2 t}$	k_2 = equilibrium rate constant (g·mg^{-1}·min^{-1})
Intraparticle Diffusion model	$Q_t = k_i t^{1/2} + C$	k_i = rate constant mg·g^{-1}·min$^{-0.5}$, C = boundary layer thickness

Furthermore, to elucidate the adsorption thermodynamics, Pb^{+2} and EBT adsorption was conducted at different temperature in the range of 25 to 40 ^{0}C with 0.8 g·L^{-1} of adsorbent was suspended in 50 mL 50 ppm Pb^{+2}/EBT solution agitated at 200 rpm for 2 h. The various thermodynamic parameters at equilibrium, including Gibb's free energy change (ΔG^0), enthalpy change (ΔH^0) and entropy change (ΔS^0) were calculated based on the adsorbate concentration C_e (mg·L^{-1}) and adsorption capacity Q_e (mg·g^{-1}) in solution in equilibrium at different temperatures.

2.4 Biosorbent regeneration

Regeneration of used JMSP biosorbent was carried with 0.2 M HNO$_3$ to desorb the sequestered Pb^{+2} and EBT, using solid/liquid ratio of 3 g·L^{-1} for 2 h. Subsequently, biosorbent separated using 0.45 μm nylon filter. The filtrate was analysed for desorbed Pb^{+2} and EBT, while separated biosorbent was washed with milli-Q water 3 times and then used for resorption study after drying in oven at 110 ^{0}C for 12 h.

2.5 Characterization of JMSP AC biosorbent

To elucidate the underlying adsorption mechanisms and active binding sites, JMSP biosorbent were characterized using a variety of physicochemical and spectroscopic approaches before and after Pb^{+2}/ EBT adsorption (i.e.,

pristine JMSP biosorbent and Pb^{+2}/EBT loaded JMSP AC). The surface electric property of JMSP biosorbent was examined by a Malvern Zetasizer (Nano Series) and pH drift method(Faria et al. 2004). Textural characterization of the JMSP AC was carried out by N_2 adsorption at 77 K using Quantachrome Autosorb IQ Surface area analyzer. The XRD diffractogram of the JMSP was recorded using $CuK\alpha$ radiation (λ = 1.54184 Å) at 30 kV and 10 mA in the range of 2θ from 5˚ to 90˚ (Bruker, Germany). The surface morphological and elemental properties of JMSP were investigated by a high-resolution scanning electron microscopy (Thermosceintific Apreo S) coupled with an EDX. Furthermore, the functional groups on the JMSP surface were identified by FTIR spectroscopy in the range of 450–4000 cm^{-1} wavenumber (perkinelmer Frontier).

3. Results and discussion

3.1 Yield and Surface electric property

The activated carbon synthesized in this study had approximate yield of 26.80 % which in agreement with the other work related to processing of JMSP for activated carbon(Treviño-Cordero et al. 2013)(Elizalde-González & Hernández-Montoya 2009). The zeta potential measurement revealed (table 4) that the surface charge for prepared activated carbon (JMSP AC), activated carbon loaded with Pb^{+2} (JMSP AC-Pb^{+2}) and EBT (JMSP AC-EBT) were -16.2 mV, -12.8 mV and -26.9 mV respectively. The result showed that the stability of JMSP AC-EBT complex was more stable than JMSP AC-Pb^{+2} complex compared to JMSP AC. The increase in zeta potential after adsorption with Pb ion indicates the binding of metal ion on the surface of biosorbent while the attachment of negatively charged functional groups on the JMSP AC surface resulted in decrease of zeta potential after EBT adsorption. The point of zero charge (pH_{PZC}) for the synthesized activated carbon was 7.42, with increasing pH the surface become more negatively charged, leading to a stronger electrostatic attraction while decrease in the pH results in more positive charge leading to stronger repulsion forces(Rambabu et al. 2020).

Table 4. The Zeta potential of JMSP AC before and after Pb^{+2} and EBT adsorption.

Material	Zeta Potential ξ (mV)
JMSP AC	-16.2
JMSP AC-Pb^{+2}	-12.8
JMSP AC-EBT	-26.9

3.2 Characterization of activated carbons

The N_2 adsorption/desorption isotherms of the prepared JMSP AC is shown in Fig. 1. According to isotherm, a progressive increase of relative pressure resulted in increased N_2 volume even at very low relative pressure (inset fig.1). The adsorption isotherm for prepared JMSP biosorbent belong to type IV isotherm according to the IUPAC classification(Sing et al. 1985), which indicates the mesoporous
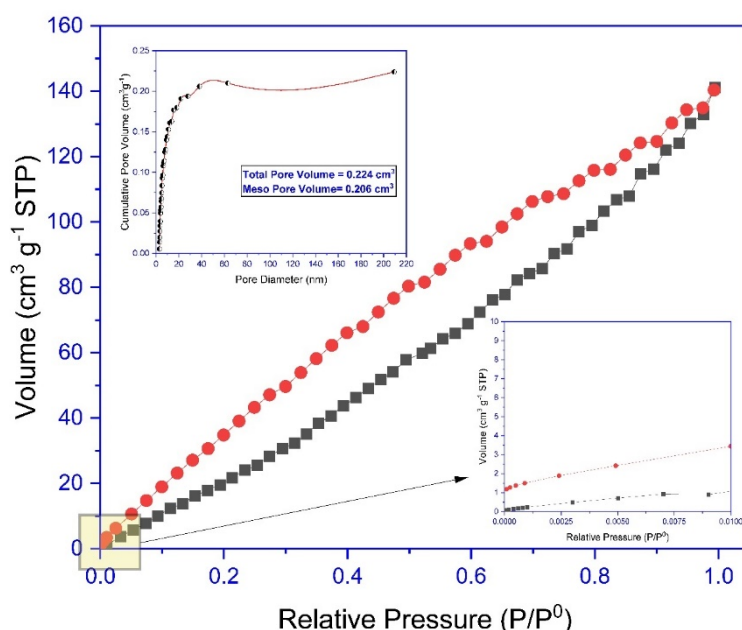

Figure 1. N_2 adsorption/desorption isotherms of the prepared JMSP AC inset shows the Pore size distribution of JMSP AC and isotherm at low relative pressure (0.010).

structure. The predominant hysteresis loop indicates the adsorption with capillary condensation(Donohue & Aranovich 1998)(Thommes et al. 2015). The development of mesoporous structure was affirmed by the pore size

distribution (inset fig.1), as shown most of the pores had sizes between 2.9 to 38 nm which is according to IUPAC classification associated with mesopores(Sing et al. 1985)(Thommes et al. 2015).

Different BET study parameters showed in table 5 revealed that, the mesopore volume was 92% of the total pore volume with surface area of 136 $m^2 \cdot g^{-1}$. The average pore size of the JMSP AC was 3.10 nm. In the literature, similar structure characteristics were reported with activated carbon prepared from plant-based materials(Danish et al. 2018)(Lima et al. 2019)(Cunha et al. 2020)(Kasperiski et al. 2018)(Salomón et al. 2021).

**Table 5**. BET study parameters of prepared JMSP AC.

	D_p (nm)	S_{BET} (m^2g^{-1})	V_T (cm^3g^{-1})	V_μ (cm^3g^{-1})	V_m (cm^3g^{-1})	V_m/V_T (%)	V_μ/V_T (%)
JMSP AC	3.10	136	0.224	0	0.206	92	0

D_p = average pore diameter, S_{BET} = BET surface area, V_T = total pore volume, V_μ = micropore volume, V_m = mesopore volume, V_m/V_T = percentage of mesopore, V_μ/V_T = percentage of micropore

The surface morphological aspects of the synthesized biosorbent by SEM are represented in figure 2. The prepared JMSP AC biosorbent (fig. 2b) observed greater surface irregularity compared to the raw *Jacaranda mimosifolia* seed pods (fig. 2a) with evenly distribution of the cavities over the surface. These pores are favourable to the
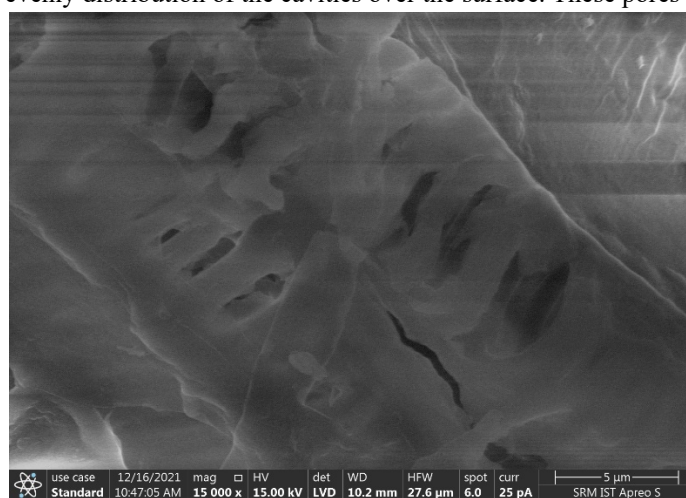
(a)
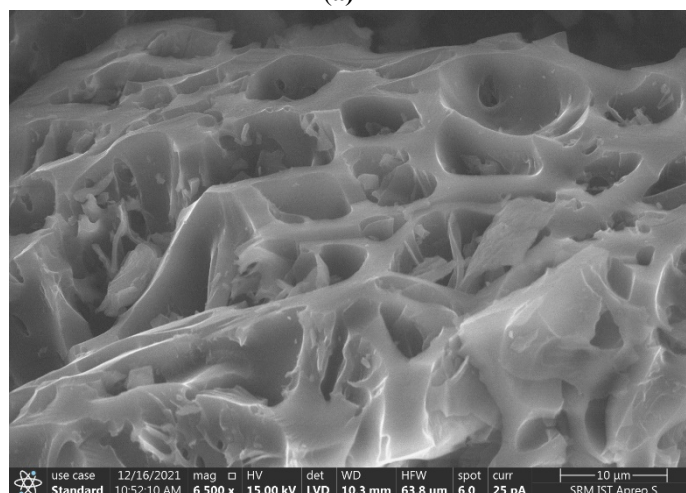
(b)

Figure 2. SEM images of (a) Raw Jacaranda mimosifolia seed pods (JMSP) (b) prepared JMSP AC biosorbent

adsorption, as they can increase the adsorption capacity of the adsorbate molecules of Pb^{+2} and EBT. After the Pb^{+2} adsorption on the biosorbent, some metal particles precipitate was observed. The elemental mapping exhibits the intense signal for Pb and O, confirmed the microprecipitation of Pb^{+2} on the surface of the biosorbent.

The XRD diffraction study reveal the crystalline property of JMSP (Fig. 3a). The broad peak at $2\theta^0$ of 8-29 is the characteristics of the various amorphous phases such as hemicellulose, lignin and amorphous cellulose of the prepared biosorbent. The distinct reflection at $2\theta^0$ of 16 and 26 along with unresolved doublet at 22

and 23 are corresponded to starch of *Jacaranda mimosifolia* seed pod biosorbent(Sandhu & Lim 2008)(Patiño-Rodríguez et al. 2020). Cellulose from the JMSP has a well-defined crystal structure with absorption peaks in XRD diffractogram at 2θ angles of 16° corresponds to crystal plane (101) and 23° (002)
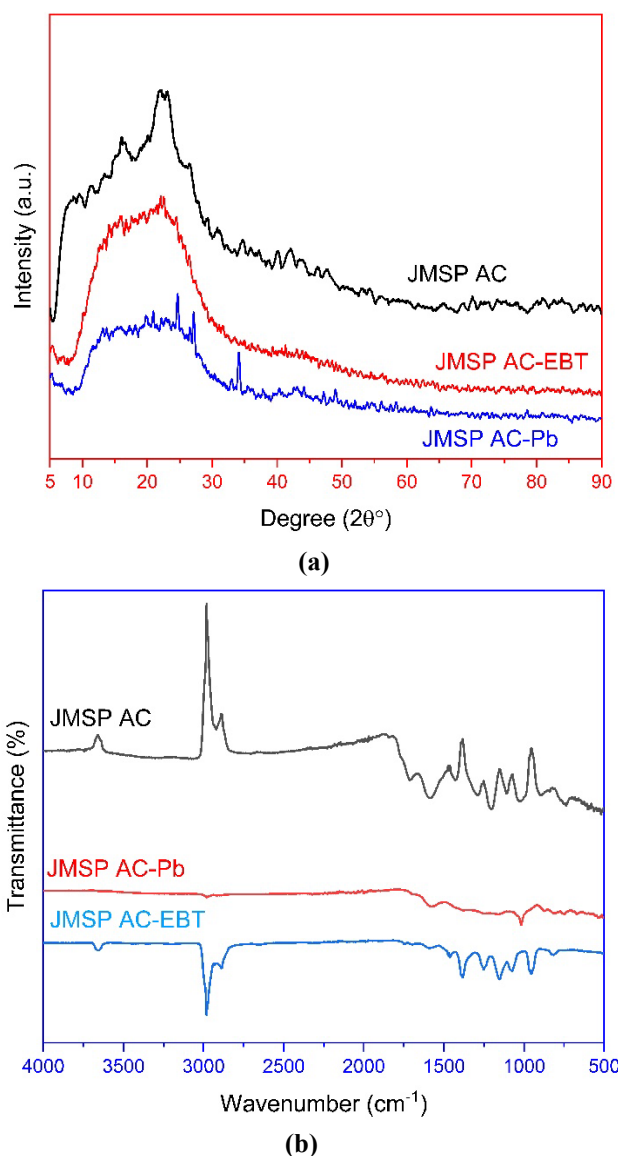

(a)

(b)

Figure 3. (a) XRD diffractogram of JMSP AC before and after Pb^{+2} and EBT adsorption. (b) FTIR Spectra of JMSP AC before and after Pb^{+2} and EBT

respectively. The presence of all the peaks in the diffractogram pattern of the JMSP AC indicated the successful formation of the desired porous carbon. It was elucidated that after the adsorption of Pb^{+2} and EBT on JMSP AC the diffractogram showed the broader and weaker reflections confirms the reduced crystallinity of JMSP AC. This should be due to the binding of JMSP AC with Pb^{+2} and EBT resulted in disorientation of the crystalline regions of JMSP AC, because of hydrogen bond breakage to prevent the disorientation of crystalline regions(Moyo et al. 2017). These amorphous regions were responsible for adsorption of Pb^{+2} and EBT on biosorbent.

The changes in various functional groups on the JMSP AC biosorbent before and after adsorption of Pb^{+2} and EBT can be seen from FTIR spectra (Fig. 3b). The complex composition of JMSP AC biosorbent could be realised from the various adsorption bands observed. The FTIR spectra of JMSP AC biosorbent exhibited broad weak adsorption bands for stretching vibration of O–H with free hydroxyl at 3660 cm^{-1}, twin sharp band at 2981 cm^{-1} and 2973 cm^{-1} with at 2924 cm^{-1} for C–H in alkanes, C=O stretch in saturated carbonyl at 1715 cm^{-1}, bending vibrations of N–H in primary amines at 1591 cm^{-1}, stretching of acyl C–O at 1286 cm^{-1} and 1206 cm^{-1}, stretching of amines C–N at 1109 cm^{-1}, C–O in primary alcohol at 1028 cm^{-1} and bending of alkene C–H at 839 cm^{-1}. This confirms the existence of various functional groups in JMSP AC, e.g., hydroxyl, amine, carboxyl and alkene. After the adsorption with Pb^{+2} and EBT on biosorbents, all such bands were removed for Pb^{+2} adsorption and weakened for EBT suggests the binding of Pb^{+2} and EBT to the functional groups(Hufton et al. 2021)(Ren et al. 2022) which

strongly favour the adsorption of pollutants on the biosorbent. Furthermore, following Pb^{+2} and EBT adsorption, the prominent peak at 2981 cm^{-1} and 2973 cm^{-1} was decreased and displaced, suggesting that hydrogen bonding may be associated with the Pb^{+2} and EBT sorption process by JMSP AC. The peak at 1591 cm^{-1} may have been caused by the JMSP AC stretching vibration, which shifted following the adsorption of Pb^{+2} and EBT, suggesting that π-π type interaction may have been involved in the adsorption process by JMSP AC.

3.3 Adsorption performance of JMSP AC for Pb^{+2} and EBT

3.3.1 Effect of pH on adsorption

It was evident that, pH of the solution plays pivotal role in adsorption studies due to its effect on the electrostatic interaction between adsorbates and adsorbents. In the present study, the effect of pH on the removal of heavy metal
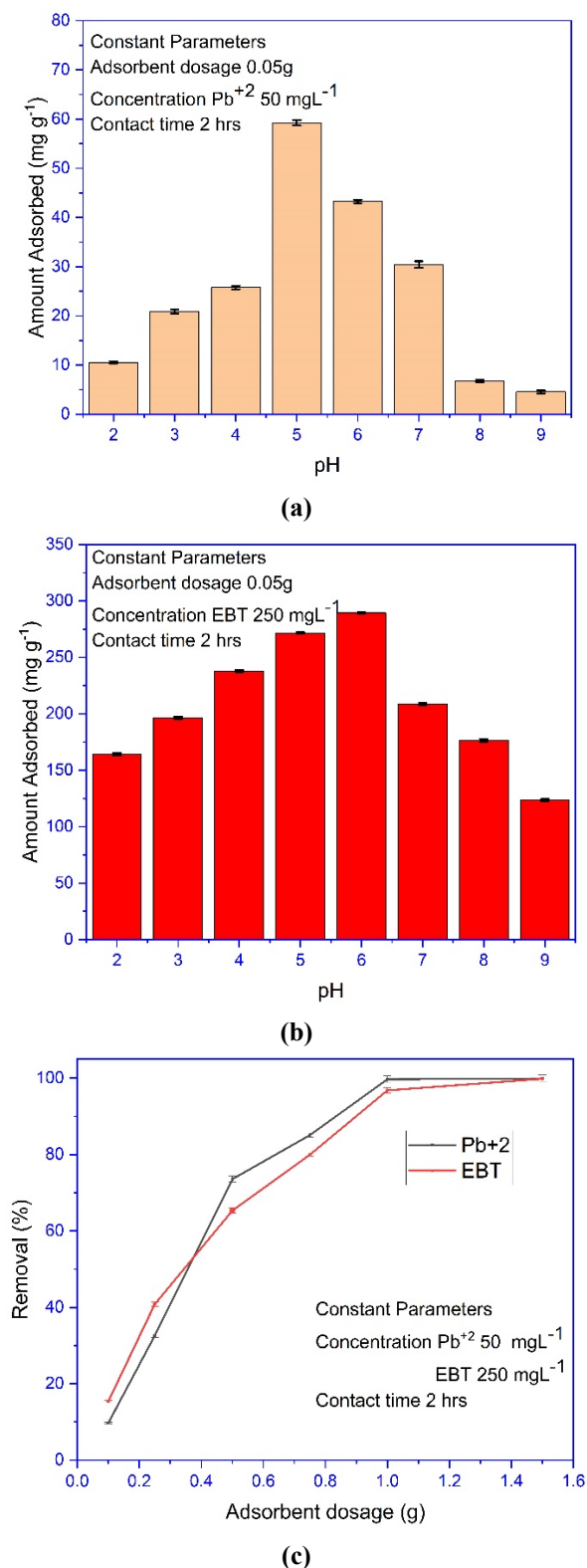

(a)

(b)

(c)

Figure 4. Effect of pH (a & b) and dosage (c) for the adsorption of Pb^{+2} and EBT on JMSP AC.

Pb^{+2} and dye EBT was determined in the EBT pH range from 2 – 9. For pH>9, under basic conditions the formation of the precipitation of salts occurred as their hydroxide can influence the adsorption process, therefore adsorption study was conducted for pH up to 9. Lead ions (Pb^{+2}) showed the maximum adsorption about 59.24 mg·L^{-1} at pH 5 (fig. 4a) and for EBT, pH 6 was found to be optimum with maximum adsorption of 289.32 mg·L^{-1} (fig. 4b).

3.3.2 Effect of dosage on adsorption

The minimum possible dosage for the optimum adsorption of Pb^{+2} and EBT was determined, the amount of biosorbent dosage was varied 0.1 g, 0.25 g, 0.50 g, 0.75 g, 1.0 g and 1.5 g in 100 ml of 50 mg·L^{-1} Pb^{+2} and 250 mg·L^{-1} EBT solution. The adsorption was increased with the amount of biosorbent dosage for the Pb^{+2} ions and EBT, which was found to be 32.62% and 40.83% at dosage of 0.25 g and reached to 85.10% and 79.96% at dosage of 0.50 g (fig. 4c). The adsorption reached to about 100% removal of metal ion Pb^{+2} and dye EBT at 1.5 g of JMSP AC, however the overall adsorption of Pb^{+2} is lower than the EBT on the biosorbent. As can be observed trend of adsorption with the adsorbent dosage, with increase in dosage the adsorption increases and reached to maximum at 1.5 g. These, observations evince that adsorption is directly proportional to the amount of the adsorbent dosage.

3.4 Adsorption isotherms

In the equilibrium study, the nonlinear isotherm models of langmuir, freundlich, temkin and Redlich- Peterson (R-P) are realized to determine the mode of adsorption and interaction between the metal ion Pb^{+2} and dye EBT. Figure 5 shows the nonlinear fitting for the above models for Pb^{+2} (fig. 5a) and EBT (fig. 5b), and table 6 shows

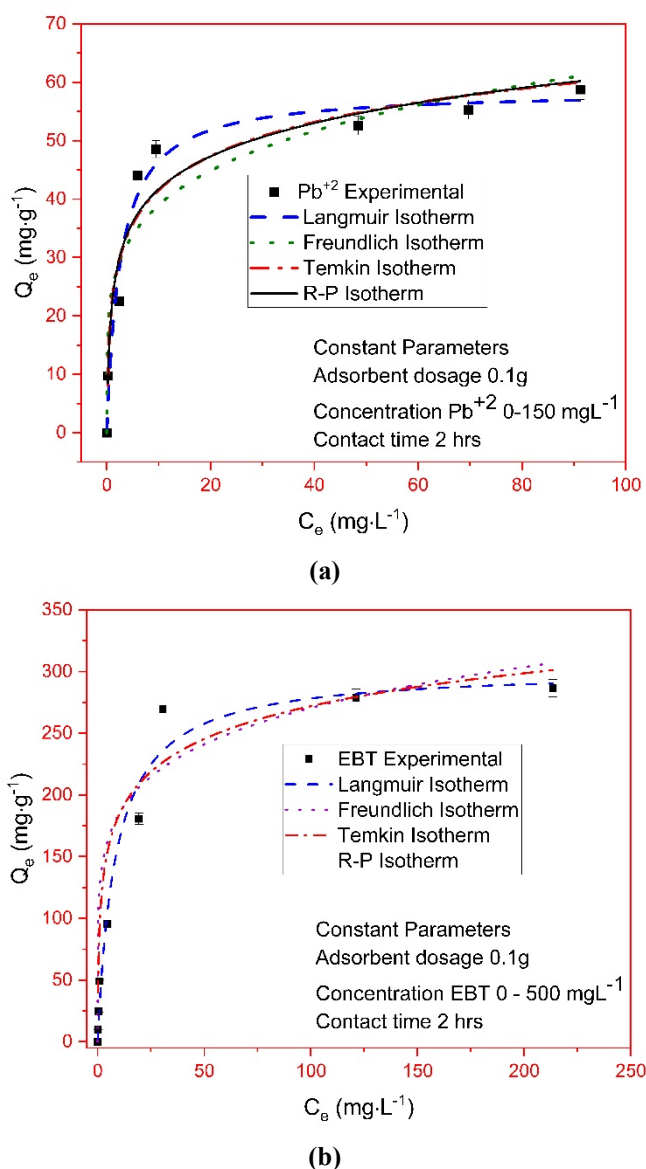**(a)**

(b)

Figure 5. Adsorption isotherm of Pb^{+2} (a) and EBT (b) adsorption on JMSP AC with nonlinear fitting to langmuir, freundlich, temkin and R-P models.

the values of constants and correlation coefficient for all four isotherm models. The maximum Pb^{+2} adsorption capacity of JMSP AC was determined to be 58.77 mg·g^{-1} and the R-P adsorption model provided the best

description (Fig. 5a, Table 6) with correlation coefficient (R^2) of 0.9998. For, EBT adsorption, the maximum adsorption capacity was 286.56 mg·g^{-1} and similar nonlinear R-P adsorption model provided the best description (Fig. 5b, Table 6) with correlation coefficient (R^2) of 0.9996. The features of langmuir and freundlich isotherms incorporated in the R-P model and it reduces to freundlich model if the value of $a_R C_e^g$ is much higher than 1.0 and approaches the langmuir model when g equals 1.0. This suggests the multilayer adsorption of Pb^{+2} and EBT on the heterogenous surface of JMSP AC.

Furthermore, a dimensionless constant; the separation factor (R_L) defined by the following relationship predicting the adsorption nature of the process.

$$R_L = \frac{1}{1+K_L C_0} \tag{5}$$

where K_L refers to Langmuir constant and C_0 is the initial concentration of adsorbate in (mg·L^{-1}). The separation factor indicates the nature of adsorption to either be irreversible ($R_L = 0$), unfavourable ($R_L > 1$), linear ($R_L = 1$) or favourable ($0 < R_L < 1$).

Table 6. Parameters for adsorption isotherm and kinetic models of Pb+2 and EBT adsorption by JMSP AC.

| Models	Parameter	Pb^{+2}	EBT
Isotherms			
Langmuir	Q_m	58.56	302.1
	K_L	0.38	0.12
	R^2	0.9762	0.9779
Freundlich	K_F	24.41	125.8
	n	4.92	6.01
	R^2	0.9106	0.8617
Temkin	A_T	14.49	12.02
	B_T	8.35	38.36
	R^2	0.9524	0.9859
Redlich-Peterson	K_R	69.65	232.66
	a_R	2.18	1.58
	g	0.86	0.87
	R^2	**0.9998**	**0.9996**
Kinetics			
Pseudo-first order	Q_e	59.51	234.28
	k_1	0.05	0.1
	R^2	**0.9945**	0.9736
Pseudo-second order	Q_e	68.26	253.39
	k_2	9.72 x 10^{-4}	6.13 x 10^{-4}
	R^2	0.9813	**0.9967**
Intraparticle Diffusion	k_i	4.17	7.95
	C	17.28	153.57
	R^2	0.7462	0.8799

(Note: Q_e - Equilibrium adsorption capacity, Q_m - Maximum adsorption capacity. Details of other parameters are referred to Table 3)

In the present study, the experimentally calculated R_L values for the adsorption of Pb^{+2} and EBT on synthesized JMSP AC were 0.0172 - 0.2083 and 0.0164 – 0.4545 respectively. These R_L values confirmed that biosorbent JMSP AC is favourable for adsorbing Pb^{+2} and EBT from water.

In addition to this, values of freundlich constant n were found to be 4.92 (1/n = 0.203) and 6.01(1/n = 0.166) for the adsorption of Pb^{+2} and EBT respectively, suggesting favourable adsorption (0<1/n<1) on the surface of synthesized biosorbent. This encourage the utilization of low cost JMSP AC for removal/recovery of heavy metals and dyes from (waste)water.

3.5 Adsorption kinetics

To determine the kinetics of Pb^{+2} and EBT adsorption on JMSP AC, different models including pseudo-first order, pseudo-second order and Intraparticle diffusion were applied. Figure 6 shows the kinetic fitting for different models, Table 6 represents the various constants for the fitted models along with the correlation coefficient. It was
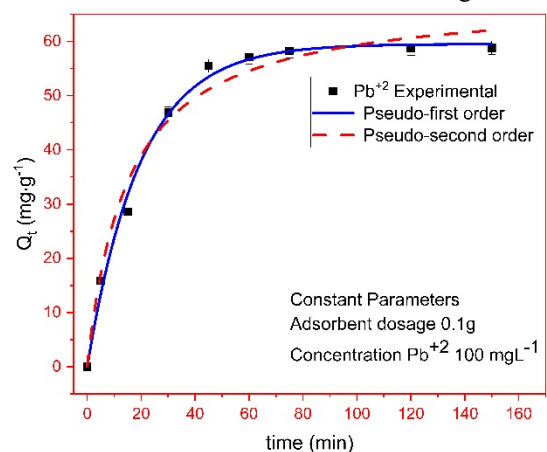
(a)
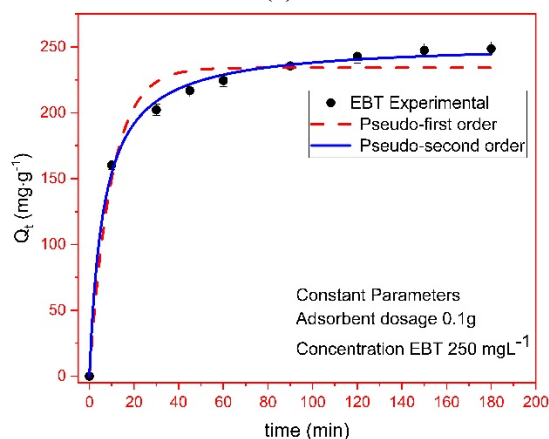
(b)
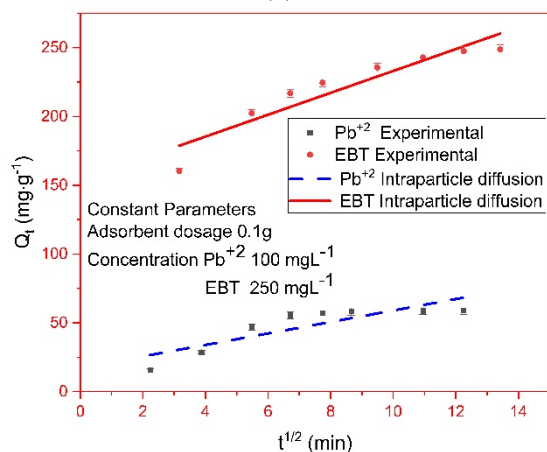
(c)

Figure 6. Adsorption kinetics of Pb^{+2} (a) and EBT (b) adsorption on JMSP AC with nonlinear fitting to pseudo-first order, pseudo-second order and Intraparticle diffusion (c) kinetic models.

found that the adsorption follows the pseudo-first order and pseudo-second order for the adsorption of Pb^{+2} (Fig 6a, Table 6) and EBT (Fig 6b, Table 6) on the synthesized JMSP AC respectively with the correlation coefficient (R^2) 0.9945 and 0.9967. The intercept C for the intraparticle diffusion (Fig 6c, Table6) for Pb^{+2} and EBT adsorption was 17.28 and 153.57 respectively, evident that the effect of boundary layer is higher for EBT adsorption than that of Pb^{+2} on the surface of biosorbent. Further, analysis of the kinetic data for intraparticle diffusion model observed that the plot does not pass through the origin suggesting that intraparticle diffusion was not the only rate-limiting step for the adsorption of Pb^{+2} and EBT on biosorbent.

The equilibria of the Pb^{+2} and EBT adsorption processes on JMSP AC were readily reached within 180 min, with 97.04% of Pb^{+2} and 90.28% of EBT adsorption reached in first 60 min (Fig. 6).

The Pb^{+2} and EBT adsorption processes have three phases: In the first phase, in the first 20 min, Pb^{+2} and EBT quickly bound to JMSP AC due to the high availability of the free surface biding sites; for second phase from 20 to 60 min, it was gradual decrease in adsorption rate and final third stage after 60 min, which characterize as equilibrium stage with slow uptake of Pb^{+2} and EBT on the biosorbent due to the less free binding sites available as a result of surface saturation of the adsorbent and decreased concentration of Pb^{+2} and EBT in the liquid phase.

3.6 Adsorption thermodynamics

The temperature (25 to 40 ^{0}C) effect on adsorption of Pb^{+2} and EBT was investigated. Thermodynamic parameters such as free energy change (ΔG^0), enthalpy (ΔH^0) and entropy (ΔS^0) were calculated according to equations.

$$\Delta G^0 = - RTlnK_d \tag{6}$$

$$K_d = \frac{Q_e}{c_e} \tag{7}$$

$$\Delta G^0 = \Delta H^0 - T\Delta S^0 \tag{8}$$

The parameter ΔH^0 and ΔS^0 were obtained from the slope and intercept of the plot lnK_d versus $1/T$. The thermodynamic parameters are given in table 7, the ΔG^0 of Pb+2 adsorption by JMSP AC biosorbent was -7.39, -5.93, -4.17 and -2.78 kJ/mol at 298, 303, 308 and 313 K, respectively. This reflects that the Pb^{+2} adsorption process became less spontaneous with increased temperature. The ΔH^0 and ΔS^0 were estimated to be -100.22 kJ/mol and -0.311 kJ/K/mol, respectively. This implies that the Pb^{+2} adsorption by JMSP AC was exothermic and reduced randomness at the solid-liquid interface of the adsorption system.

For EBT adsorption, the ΔG^0 was -9.11, -7.10, -5.39 and -3.67 kJ/mol at 298, 303, 308 and 313 K, respectively; indicates the reduced adsorption spontaneity at higher temperature. the ΔH^0 and ΔS^0 were estimated to be -116.66 kJ/mol and -0.361 kJ/K/mol, respectively. The decreased adsorption of Pb^{+2} and EBT by biosorbent at higher temperature could reduce the thickness of thermal boundary for the adsorbed Pb^{+2}/EBT leads to the escape from the JMSP AC surface back into the bulk solution (Rambabu et al., 2020). This probably indicates a poor interplay between adsorbate and various surface functionalities of JMSP AC.

Table 7. The thermodynamic parameters of Pb+2 and EBT adsorption by JMSP AC biosorbent.

	ΔG^0 (kJ/mol)	ΔH^0 (kJ/mol)	ΔS^0 (kJ/K/mol)
Pb^{+2} adsorption			
298 K	-7.39	-100.22	-0.311
303 K	-5.93		
308 K	-4.17		
313 K	-2.78		
EBT adsorption			
298 K	-9.11	-116.66	-0.361
303 K	-7.10		
308 K	-5.39		
313 K	-3.67		

The adsorption mechanism of Pb^{+2} and EBT on JMSP AC biosorbents were explored by examining experimental data through various kinetic models including pseudo-first order, pseudo-second order, and intraparticle diffusion. The proton quantity could influence the adsorption for Pb^{+2} and EBT, suggesting the surface-active regions on JMSP AC. The various interaction between surface of JMSP AC and Pb^{+2}/EBT resulted in adsorption including surface complexation, microprecipitation and electrostatic attraction (Fig 7)
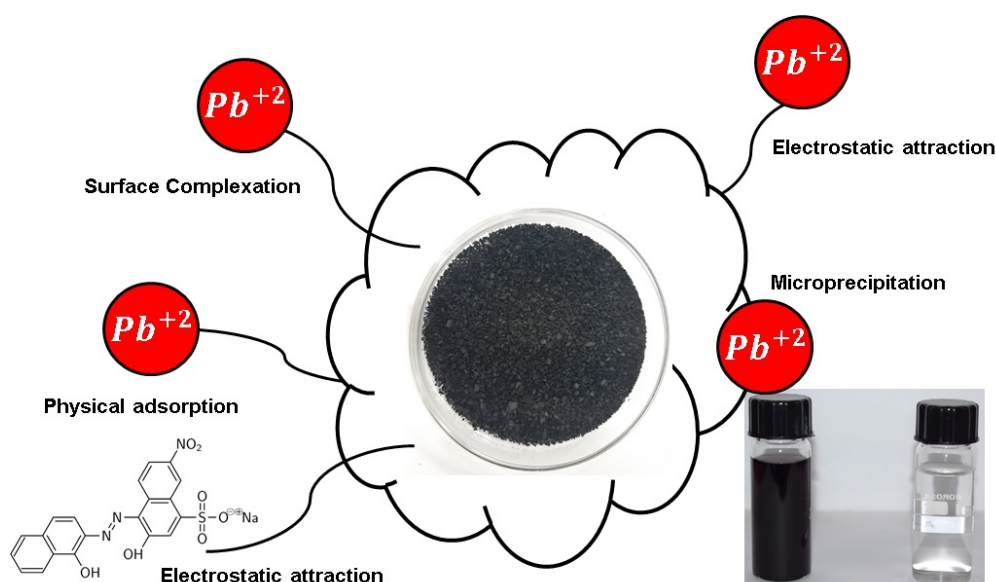
Figure 7. Schematics of Adsorption mechanism of Pb^{+2} and EBT on JMSP AC

3.7 Regeneration of biosorbent

In the practical application, the regeneration ability of biosorbent along with stability are usually important factors, which was investigated through six consecutive adsorption-desorption cycles (fig. 8) using 0.2 M HNO$_3$ as effective eluting agents for regeneration of the JMSP AC biosorbents. However, biosorbents based on plant biomass are low cost and readily available and may not be recycled. As can be seen, the adsorption efficiency decreased with an increasing numbers of regeneration cycles i.e., for Pb^{+2} efficiency was reduced from 83% to 68 % during first three cycles and further reduced to 39% after sixth regeneration cycle, whereas for EBT efficiency was reduced from 92% to 85 % and further reduced to 12% at the end of sixth regeneration cycle. This indicates that the biosorbent could be recycled with proper treatments. To optimize regeneration process the eluting agents solution stirred at 50-100 rpm for 120 minutes at 298.15 K, this helps to minimize pickling the surface of JMSP AC which facilitate to reduce the decline in adsorption efficiency over the cycles.
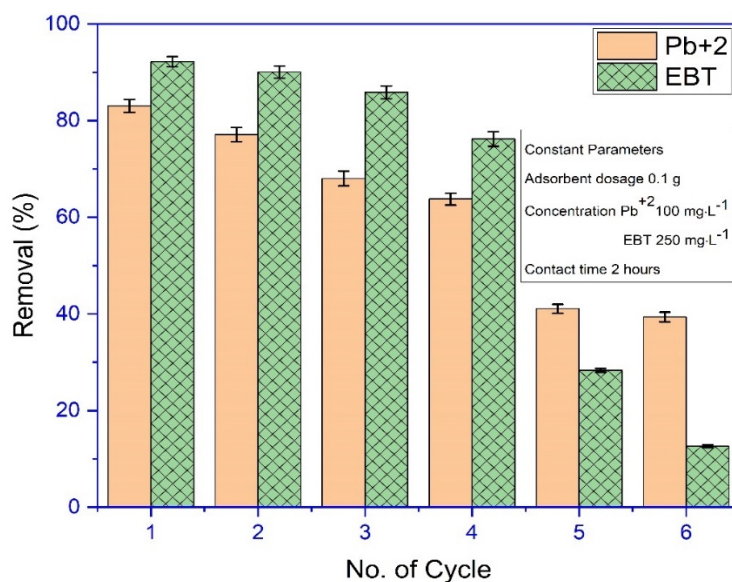

Figure 8. Sequential adsorption- desorption cycles of the prepared JMSP AC for regeneration.

3.8 Comparative Studies

Different biosorbents synthesized from lignocellulosic biomass were applied for the removal of heavy metal ion Pb^{+2} and dye EBT from water. Table 8 shows the maximum adsorption capacity (Q$_m$) of different adsorbents for removal of Pb^{+2} and EBT. The comparative adsorptions as shown in table 8 depict that the synthesized biosorbent JMSP AC is much more efficient compared to the other adsorbents. The previous study had various limitation in

terms of cost-effectiveness, scale-up, energy consumption, regeneration potential, reproducibility, implementation in resource constrained regions for large scale water treatment and environmental sustainability. As major

Table 8. The adsorbent JMSP AC comparison of adsorption capacities for Pb+2 and EBT with different adsorbents.

Sr.No.	Pollutants	Adsorbents	Q_m (mg·g^{-1})	Ref.
1	Pb^{+2}	Kenaf based activated carbon (KAC)	11.236	(Mandal et al. 2021)
2		activated carbon (date palm fiber)	29.859	(Melliti et al. 2023)
3		Activated carbon (Theobroma-Tithonia)	46.95	(Eletta et al. 2023)
4		f-activated carbon (palm tree)	4.112	(Bumajdad & Hasila 2023)
5		activated carbon (red algae-Gracilaria changii)	36.231	(Isam et al. 2024)
6		Activated carbon (Teff Straw)	42.97	(Beyan et al. 2024)
7		Activated carbon-sodium alginate-oxalate gel particles	53.04	(Li et al. 2024)
8		activated carbon (banana peel)	6	(Mkilima et al. 2024)
9		Activated Carbon (Cypress Fruit)	56.18	(Al-Ma'abreh et al. 2024)
10		kenaf-core activated carbon	12.7	(Mandal et al. 2021)
11		Chemically activated Jute	25	(Aziz et al. 2019)
12		Jacaranda mimosifolia Seed pod Activated Carbon	58.77	present work
13	EBT	Activated carbon (Spartium junceum)	261.36	(Abiza et al. 2024)
14		Chitosan (Shrimp shell)	162.3	(Khnifira et al. 2021)
15		Activated carbon (Datura metel seeds)	154.5	(Ali et al. 2022)
16		biochar (giant reed)	9.06	(Abdu et al. 2024)
17		Activated Carbon (Waste Hemp Cannabis sativa L)	14.025	(El Mansouri et al. 2022)
18		graphene (wheat straw)	146.2	(Sadeghi et al. 2021)
19		Activated carbon (typha grass)	47.619	(Ayuba & Sani 2022)
20		graphene oxide/activated carbon (Carica papaya seeds)	51.84	(Rath et al. 2024)
21		Nano Carbon (Morus Nigra (Mulberry) Stem)	192.308	(Ahmed et al. 2024)
22		Activated Carbon (Pepper Stalks)	55.56	(DOLAŞ 2023)
23		Jacaranda mimosifolia Seed pod Activated Carbon	286.56	present work

synthesis processes used toxic chemicals in their production cycle ((Melliti et al. 2023), (Eletta et al. 2023), (Bumajdad & Hasila 2023), (Beyan et al. 2024), (Isam et al. 2024), (Al-Ma'abreh et al. 2024), (Aziz et al. 2019), (Abiza et al. 2024), (Ali et al. 2022), (Ayuba & Sani 2022), (El Mansouri et al. 2022), (Rath et al. 2024), (Sadeghi

et al. 2021)) for activated carbon including chemicals used in pre and post treatment steps. The scalability and reproducibility of disclosed processes has limited scope as non-sufficient disclosure of entire production process ((Mandal et al. 2021), (Melliti et al. 2023), (Eletta et al. 2023), (Bumajdad & Hasila 2023), (Isam et al. 2024), (Mkilima et al. 2024), (Ali et al. 2022), (El Mansouri et al. 2022)), this prone to the hurdle in adaptation of production processes at commercial scale. Major constrain for implementation of large scale production of activated carbon includes availability of energy and emission of huge amount of greenhouse gases (GHG) as major production processes were very energy intensive, these processes had very high specific energy consumption in terms of kilo watt hours (KWH) per kilogram of activated carbon produces which leads to high GHG footprint. Contrast to above limitations our single step green synthesis process addresses major constrain for its adaptability at industrial scale production, first our process did not require any environmentally hazardous chemicals, secondly required very less energy compared previously reported processes and finally disclosed production process could easily scale-up and reproduce as our study has sufficient disclosure of the entire production process. The cost-effectiveness of our single step green synthesis process made it easy to adopt for large scale water treatment facility for environmental sustainability. Thus, our study linked with availability and sustainable management of water (SDG6), sustainable consumption of natural resources (SDG12) for production of Activated carbon with Smaller environmental footprint leads to the reduced GHG Emissions (SDG13).

Based on current study, we learned distinct reasons for the high adsorption capacities of the synthesized JMSP AC.

1) The single step synthesis method produces several types of active sites.
2) Surface hydroxyl groups produce the surface complexation between contaminants.
3) Electrostatic attraction, co-exchanges, microprecipitation, surface diffusion occur between Pb^{+2} and EBT and prepared biosorbent.
4) The porous architecture of the synthesized biosorbent is favourable to the adsorption of various contaminants.
5) The adopted single step synthesis method produces abundant transformation sites responsible to introduces physiochemical partition and stacking of sites to adsorb contaminant molecules.

4. Conclusion

In summary, we investigated novel and scalable synthesis of JMSP AC and its application for the removal of contaminants from water and wastewater. The synthesized biosorbent, a waste to resource product, manifested efficient adsorption of Pb^{+2} and EBT (Q_m of 58.77 mg-Pb^{+2}/g and 286.56 mg-EBT/g). The adopted single step synthesis method is more efficient and eco-friendlier compared to expensive conventional energy intensive production and treatment processes. The binding sites for Pb^{+2} and EBT were identified as hydroxyl, amine, ether and carboxyl groups. The underlying adsorption mechanism comprising electrostatic attraction, microprecipitation, diffusion and complexation. The mechanism provides the understanding of interactions between water pollutants and biosorbents. This study reveals the single step eco-friendly and scalable synthesis method for producing activated carbon (biosorbent) for removal of heavy metal and dye from water.

Author Contributions: Vishal Haribhai Patel: Conceptualization, Methodology, Data curation, Visualization, Investigation, Validation, Writing- Original draft preparation, Reviewing and Editing **Abdul Gani:** Conceptualization, Supervision, Writing- Reviewing and Editing **Anamika Paul:** Conceptualization, Supervision, Writing- Reviewing and Editing

Declaration of Competing Interest
The authors declare that they have no known competing financial interests or personal relationships that could have appeared to influence the work reported in this paper.

REFERENCES

Abdu, M., Babaee, S., Worku, A., Msagati, T.A.M. and Nure, J.F., 2024. The development of Giant reed biochar for adsorption of Basic Blue 41 and Eriochrome Black T. azo dyes from wastewater. *Scientific Reports*, 14(1), p.18320. https://doi.org/10.1038/s41598-024-67997-5.

Abiza, A., Reffas, A., Boubaker, H., Ben Arfi, R., Ghorbel, D., Rafique, M., Bachirou, G.L. and Ghorbal, A., 2024. Comparative analysis of EBT dye removal using *Spartium junceum* and derived activated carbon: experimental and DFT insights. *International Journal of Environmental Analytical Chemistry*, pp.1–27. https://doi.org/10.1080/03067319.2024.2391953.

Agroforestree database : a tree reference and selection guide, version 4.0 | CiNii Research, n.d. https://cir.nii.ac.jp/crid/1571417126302995328.

Ahmed, M., Ismaeel, S. and Al-Hyali, E., 2024. Equilibrium and Thermodynamic Studies for the Removal of Eriochrome Black T dye from its Aqueous Solutions using Nano Carbon Prepared from *Morus Nigra* (Mulberry) Stem through two Stages of Carbonization. *Journal of Education and Science*, 33(2), pp.81–97. https://doi.org/10.33899/edusj.2024.148527.1445.

Ali, H., Khan, E. and Ilahi, I., 2019. Environmental chemistry and ecotoxicology of hazardous heavy metals: Environmental persistence, toxicity, and bioaccumulation. *Journal of Chemistry*, pp.1–14. https://doi.org/10.1155/2019/6730305.

Ali, J., Bakhsh, E.M., Hussain, N., Bilal, M., Akhtar, K., Fagieh, T.M., Danish, E.Y., Asiri, A.M., Su, X. and Khan, S.B., 2022. A new biosource for synthesis of activated carbon and its potential use for removal of methylene blue and eriochrome black T from aqueous solutions. *Industrial Crops and Products*, 179, p.114676. https://doi.org/10.1016/j.indcrop.2022.114676.

Al-Ma'abreh, A.M., AlKhabbas, M., Alawaideh, S., Hussein-Al-Ali, S.H., Hmedat, D.A., Edris, G., Abuassaf, R.A. and Hamed, M.A., 2024. Investigation of kinetics, thermodynamics, and isotherms of the simultaneous removal of heavy metal ions by activated carbon from cypress fruit. *Adsorption Science & Technology*, 42, pp.1-15. https://doi.org/10.1177/02636174241256853.

Alonso-Magdalena, P., Tudurí, E., Marroquí, L., Quesada, I., Sargis, R.M. and Nadal, A., 2019. Toxic Effects of Common Environmental Pollutants in Pancreatic β-Cells and the Onset of Diabetes Mellitus. *Encyclopedia of Endocrine Diseases*, pp.764–775. https://doi.org/10.1016/B978-0-12-801238-3.64325-8.

Ayuba, A.M. and Sani, M., 2022. Removal of Eriochrome Black T dye from aqueous solution using base activated typha grass (*Typha latifolia*) as an adsorbent. *Bayero Journal of Pure and Applied Sciences*, 15(1), pp.95–104. https://doi.org/10.4314/bajopas.v15i1.13.

Azari, A., Noorisepehr, M., Dehganifard, E., Karimyan, K., Hashemi, S.Y., Kalhori, E.M., Norouzi, R., Agarwal, S. and Gupta, V.K., 2019. Experimental design, modeling and mechanism of cationic dyes biosorption on to magnetic chitosan-lutaraldehyde composite. *International Journal of Biological Macromolecules*, 131, pp.633–645. https://doi.org/10.1016/J.IJBIOMAC.2019.03.058.

Aziz, M.A., Chowdhury, I.R., Mazumder, M.A.J. and Chowdhury, S., 2019. Highly porous carboxylated activated carbon from jute stick for removal of Pb2+ from aqueous solution. *Environmental Science and Pollution Research*, 26(22), pp.22656–22669. https://doi.org/10.1007/S11356-019-05556-6.

Bello, K., Sarojini, B.K., Narayana, B., Rao, A. and Byrappa, K., 2018. A study on adsorption behavior of newly synthesized banana pseudo-stem derived superabsorbent hydrogels for cationic and anionic dye removal from effluents. *Carbohydrate Polymers*, 181, pp.605–615. https://doi.org/10.1016/J.CARBPOL.2017.11.106.

Beyan, S.M., Ambio, T.A., Sundramurthy, V.P., Gomadurai, C. and Getahun, A.A., 2024. Adsorption Phenomenon for Removal of Pb(II) via Teff Straw based Activated Carbon Prepared by Microwave-Assisted Pyrolysis: Process Modelling, Statistical Optimisation, Isotherm, Kinetics, and Thermodynamic Studies. *International Journal of Environmental Analytical Chemistry*, 104(4), pp.916–937. https://doi.org/10.1080/03067319.2022.2026942.

Bumajdad, A. and Hasila, P., 2023. Surface modification of date palm activated carbonaceous materials for heavy metal removal and CO2 adsorption. *Arabian Journal of Chemistry*, 16(1), p.104403. https://doi.org/10.1016/j.arabjc.2022.104403.

Chen, Q., Yao, Y., Li, X., Lu, J., Zhou, J. and Huang, Z., 2018. Comparison of heavy metal removals from aqueous solutions by chemical precipitation and characteristics of precipitates. *Journal of Water Process Engineering*, 26, pp.289–300. https://doi.org/10.1016/J.JWPE.2018.11.003.

Cunha, M.R., Lima, E.C., Lima, D.R., da Silva, R.S., Thue, P.S., Seliem, M.K., Sher, F., dos Reis, G.S. and Larsson, S.H., 2020. Removal of captopril pharmaceutical from synthetic pharmaceutical-industry wastewaters: Use of activated carbon derived from Butia catarinensis. *Journal of Environmental Chemical Engineering*, 8(6), p.104506. https://doi.org/10.1016/j.jece.2020.104506.

Danish, M., Ahmad, T., Hashim, R., Said, N., Akhtar, M.N., Mohamad-Saleh, J. and Sulaiman, O., 2018. Comparison of surface properties of wood biomass activated carbons and their application against rhodamine B and methylene blue dye. *Surfaces and Interfaces*, 11, pp.1–13. https://doi.org/10.1016/J.SURFIN.2018.02.001.

Dobrowolski, R., Krzyszczak, A., Dobrzyńska, J., Podkościelna, B., Zięba, E., Czemierska, M., Jarosz-Wilkołazka, A. and Stefaniak, E.A., 2019. Extracellular polymeric substances immobilized on microspheres for removal of heavy metals from aqueous environment. *Biochemical Engineering Journal*, 143, pp.202–211. https://doi.org/10.1016/J.BEJ.2019.01.004.

Doggaz, A., Attoura, A., le Page Mostefa, M., Côme, K., Tlili, M. and Lapicque, F., 2019. Removal of heavy metals by electrocoagulation from hydrogenocarbonate-containing waters: Compared cases of divalent iron and zinc cations. *Journal of Water Process Engineering*, 29, p.100796. https://doi.org/10.1016/j.jwpe.2019.100796.

DOLAŞ, H., 2023. The Adsorption of Eriochrome Black T onto the Activated Carbon Produced from Pepper Stalks. *Journal of Engineering Technology and Applied Sciences*, 8(2), pp.107–118. https://doi.org/10.30931/jetas.1145856.

Donohue, M.D. and Aranovich, G.L., 1998. Adsorption Hysteresis in Porous Solids. *Journal of Colloid and Interface Science*, 205(1), pp.121–130. https://doi.org/10.1006/JCIS.1998.5639.

Du, W.N. and Chen, S.T., 2018. Photo- and chemocatalytic oxidation of dyes in water. *Journal of Environmental Management*, 206, pp.507–515. https://doi.org/10.1016/J.JENVMAN.2017.10.042.

Eletta, O.A.A., Ayandele, F.O. and Ighalo, J.O., 2023. Adsorption of Pb(II) and Fe(II) by mesoporous composite activated carbon from Tithonia diversifolia stalk and Theobroma cacao pod. *Biomass Conversion and Biorefinery*, 13(11), pp.9831–9840. https://doi.org/10.1007/s13399-021-01699-0.

Elizalde-González, M.P. and Hernández-Montoya, V., 2009. Use of Wide-Pore Carbons to Examine Intermolecular Interactions during the Adsorption of Anthraquinone Dyes from Aqueous Solution: *Adsorption Science & Technology*, 27(5), pp.447–459. https://doi.org/10.1260/0263-6174.27.5.447.

Faria, P.C.C., Órfão, J.J.M. and Pereira, M.F.R., 2004. Adsorption of anionic and cationic dyes on activated carbons with different surface chemistries. *Water Research*, 38(8), pp.2043–2052. https://doi.org/10.1016/J.WATRES.2004.01.034.

Feng, Y., Yang, S., Xia, L., Wang, Z., Suo, N., Chen, H., Long, Y., Zhou, B. and Yu, Y., 2019. In-situ ion exchange electrocatalysis biological coupling (i-IEEBC) for simultaneously enhanced degradation of organic pollutants and heavy metals in electroplating wastewater. *Journal of Hazardous Materials*, 364, pp.562–570. https://doi.org/10.1016/J.JHAZMAT.2018.10.068.

Ghobashy, M.M. and Elhady, M.,. A., 2017. pH-sensitive wax emulsion copolymerization with acrylamide hydrogel using gamma irradiation for dye removal. *Radiation Physics and Chemistry*, 134, pp.47–55. https://doi.org/10.1016/J.RADPHYSCHEM.2017.01.021.

Gupta, N.K., Gupta, A., Ramteke, P., Sahoo, H. and Sengupta, A., 2019. Biosorption-a green method for the preconcentration of rare earth elements (REEs) from waste solutions: A review. *Journal of Molecular Liquids*, 274, pp.148–164. https://doi.org/10.1016/J.MOLLIQ.2018.10.134.

Gupta, N.K., Sengupta, A., Gupta, A., Sonawane, J.R. and Sahoo, H., 2018. Biosorption-an alternative method for nuclear waste management: A critical review. *Journal of Environmental Chemical Engineering*, 6(2), pp.2159–2175. https://doi.org/10.1016/J.JECE.2018.03.021.

Hosseini, S.A., Vossoughi, M., Mahmoodi, N.M. and Sadrzadeh, M., 2018. Efficient dye removal from aqueous solution by high-performance electrospun nanofibrous membranes through incorporation of SiO2 nanoparticles. *Journal of Cleaner Production*, 183, pp.1197–1206. https://doi.org/10.1016/J.JCLEPRO.2018.02.168.

Hou, T., Du, H., Yang, Z., Tian, Z., Shen, S., Shi, Y., Yang, W. and Zhang, L., 2019. Flocculation of different types of combined contaminants of antibiotics and heavy metals by thermo-responsive flocculants with various architectures. *Separation and Purification Technology*, 223, pp.123–132. https://doi.org/10.1016/J.SEPPUR.2019.04.068.

Hufton, J., Harding, J., Smith, T. and Romero-González, M.E., 2021. The importance of the bacterial cell wall in uranium(VI) biosorption. *Physical Chemistry Chemical Physics*, 23(2), pp.1566–1576. https://doi.org/10.1039/D0CP04067C.

Isam, M., Baloo, L., Chabuk, A., Majdi, A. and Al-Ansari, N., 2024. Optimization and modelling of Pb (II) and Cu (II) adsorption onto red algae (*Gracilaria changii*)-based activated carbon by using response surface methodology. *Biomass Conversion and Biorefinery*, 14(15), pp.16799–16818. https://doi.org/10.1007/s13399-023-04150-8.

Jacob, J.M., Karthik, C., Saratale, R.G., Kumar, S.S., Prabakar, D., Kadirvelu, K. and Pugazhendhi, A., 2018. Biological approaches to tackle heavy metal pollution: A survey of literature. *Journal of Environmental Management*, 217, pp.56–70. https://doi.org/10.1016/J.JENVMAN.2018.03.077.

Kasperiski, F.M., Lima, E.C., Umpierres, C.S., dos Reis, G.S., Thue, P.S., Lima, D.R., Dias, S.L.P., Saucier, C. and da Costa, J.B., 2018. Production of porous activated carbons from *Caesalpinia ferrea* seed pod wastes: Highly efficient removal of captopril from aqueous solutions. *Journal of Cleaner Production*, 197, pp.919–929. https://doi.org/10.1016/J.JCLEPRO.2018.06.146.

Kavitha, E., Sowmya, A., Prabhakar, S., Jain, P., Surya, R. and Rajesh, M.P., 2019. Removal and recovery of heavy metals through size enhanced ultrafiltration using chitosan derivatives and optimization with response surface modeling. *International Journal of Biological Macromolecules*, 132, pp.278–288. https://doi.org/10.1016/J.IJBIOMAC.2019.03.128.

Khnifira, M., Boumya, W., Abdennouri, M., Sadiq, M., Achak, M., Serdaroğlu, G., Kaya, S., Şimşek, S. and Barka, N., 2021. A combined molecular dynamic simulation, DFT calculations, and experimental study of the eriochrome black T dye adsorption onto chitosan in aqueous solutions. *International Journal of Biological Macromolecules*, 166, pp.707–721. https://doi.org/10.1016/j.ijbiomac.2020.10.228.

Krstić, V., Urošević, T. and Pešovski, B., 2018. A review on adsorbents for treatment of water and wastewaters containing copper ions. *Chemical Engineering Science*, 192, pp.273–287. https://doi.org/10.1016/J.CES.2018.07.022.

Li, R., Cao, X., Fan, X., Shi, J., Meng, B., Zhang, J., Wang, Y., Du, J., Deng, X. and Zheng, C., 2024. Study of the Factors Influencing the Adsorption of Heavy Metal Pollutants in Water by Activated Carbon Gel Particles. *Journal of Environmental Engineering*, 150(7). https://doi.org/10.1061/JOEEDU.EEENG-7606.

Lima, D.R., Hosseini-Bandegharaei, A., Thue, P.S., Lima, E.C., de Albuquerque, Y.R.T., dos Reis, G.S., Umpierres, C.S., Dias, S.L.P. and Tran, H.N., 2019. Efficient acetaminophen removal from water and hospital effluents treatment by activated carbons derived from Brazil nutshells. *Colloids and Surfaces A: Physicochemical and Engineering Aspects*, 583, p.123966. https://doi.org/10.1016/j.colsurfa.2019.123966.

Liu, J., Hu, C. and Huang, Q., 2019. Adsorption of Cu2+, Pb2+, and Cd2+ onto oiltea shell from water. *Bioresource Technology*, 271, pp.487–491. https://doi.org/10.1016/J.BIORTECH.2018.09.040.

M Mostafa, N., A Eldahshan, O. and B Singab, A.N., 2014. The Genus Jacaranda (*Bignoniaceae*): An Updated Review. *Pharmacognosy Communication*, 4(3), pp.31–39. https://doi.org/10.5530/PC.2014.3.3.

Madeła, M. and Skuza, M., 2021. Towards a Circular Economy: Analysis of the Use of Biowaste as Biosorbent for the Removal of Heavy Metals. *Energies,* 14(17), pp.5427–5442. https://doi.org/10.3390/EN14175427.

Mandal, S., Calderon, J., Marpu, S.B., Omary, M.A. and Shi, S.Q., 2021. Mesoporous activated carbon as a green adsorbent for the removal of heavy metals and Congo red: Characterization, adsorption kinetics, and isotherm studies. *Journal of Contaminant Hydrology*, 243, p.103869. https://doi.org/10.1016/j.jconhyd.2021.103869.

El Mansouri, F., Pelaz, G., Morán, A., Da Silva, J.C.G.E., Cacciola, F., El Farissi, H., Tayeq, H., Zerrouk, M.H. and Brigui, J., 2022. Efficient Removal of Eriochrome Black T Dye Using Activated Carbon of Waste Hemp (*Cannabis sativa L.*) Grown in Northern Morocco Enhanced by New Mathematical Models. *Separations*, 9(10), p.283. https://doi.org/10.3390/separations9100283.

Melliti, A., Yılmaz, M., Sillanpää, M., Hamrouni, B. and Vurm, R., 2023. Low-cost date palm fiber activated carbon for effective and fast heavy metal adsorption from water: Characterization, equilibrium, and kinetics studies. *Colloids and Surfaces A: Physicochemical and Engineering Aspects*, 672, p.131775. https://doi.org/10.1016/j.colsurfa.2023.131775.

Mkilima, T., Zharkenov, Y., Abduova, A., Sarypbekova, N., Kudaibergenov, N., Sakanov, K., Zhukenova, G., Omarov, Z., Sultanbekova, P. and Kenzhaliyeva, G., 2024. Utilization of banana peel-derived activated carbon for the removal of heavy metals from industrial wastewater. *Case Studies in Chemical and Environmental Engineering*, 10, p.100791. https://doi.org/10.1016/j.cscee.2024.100791.

Mohammed, N.A.S., Abu-Zurayk, R.A., Hamadneh, I. and Al-Dujaili, A.H., 2018. Phenol adsorption on biochar prepared from the pine fruit shells: Equilibrium, kinetic and thermodynamics studies. *Journal of Environmental Management*, 226, pp.377–385. https://doi.org/10.1016/J.JENVMAN.2018.08.033.

Moyo, M., Pakade, V.E. and Modise, S.J., 2017. Biosorption of lead(II) by chemically modified *Mangifera indica* seed shells: Adsorbent preparation, characterization and performance assessment. *Process Safety and Environmental Protection*, 111, pp.40–51. https://doi.org/10.1016/J.PSEP.2017.06.007.

Napoli, M., Cecchi, S., Grassi, C., Baldi, A., Zanchi, C.A. and Orlandini, S., 2019. Phytoextraction of copper from a contaminated soil using arable and vegetable crops. *Chemosphere*, 219, pp.122–129. https://doi.org/10.1016/J.CHEMOSPHERE.2018.12.017.

Nemati, M., Hosseini, S.M. and Shabanian, M., 2017. Novel electrodialysis cation exchange membrane prepared by 2-acrylamido-2-methylpropane sulfonic acid; heavy metal ions removal. *Journal of Hazardous Materials*, 337, pp.90–104. https://doi.org/10.1016/J.JHAZMAT.2017.04.074.

Özdemir, S., Mohamedsaid, S.A., Kılınç, E. and Soylak, M., 2019. Magnetic solid phase extractions of Co(II) and Hg(II) by using magnetized C. micaceus from water and food samples. *Food Chemistry*, 271, pp.232–238. https://doi.org/10.1016/J.FOODCHEM.2018.07.067.

Patiño-Rodríguez, O., Agama-Acevedo, E., Ramos-Lopez, G. and Bello-Pérez, L.A., 2020. Unripe mango kernel starch: Partial characterization. *Food Hydrocolloids*, 101, p.105512. https://doi.org/10.1016/j.foodhyd.2019.105512.

Qiu, M. and He, C., 2019. Efficient removal of heavy metal ions by forward osmosis membrane with a polydopamine modified zeolitic imidazolate framework incorporated selective layer. *Journal of Hazardous Materials*, 367, pp.339–347. https://doi.org/10.1016/J.JHAZMAT.2018.12.096.

Que, W., Zhou, Y. hui, Liu, Y. guo, Wen, J., Tan, X. fei, Liu, S. jia and Jiang, L. hua, 2019. Appraising the effect of in-situ remediation of heavy metal contaminated sediment by biochar and activated carbon on Cu immobilization and microbial community. *Ecological Engineering*, 127, pp.519–526. https://doi.org/10.1016/J.ECOLENG.2018.10.005.

Ragsac, A.C., Farias-Singer, R., Freitas, L.B., Lohmann, L.G. and Olmstead, R.G., 2019. Phylogeny of the Neotropical tribe Jacarandeae (Bignoniaceae). *American Journal of Botany*, 106(12), pp.1589–1601. https://doi.org/10.1002/AJB2.1399.

Rai, D. and Sinha, S., 2022. Research trends in the development of anodes for electrochemical oxidation of wastewater. *Reviews in Chemical Engineering,* 39(5), pp. 807–855. https://doi.org/10.1515/revce-2021-0067

Rambabu, K., Bharath, G., Banat, F. and Show, P.L., 2020. Biosorption performance of date palm empty fruit bunch wastes for toxic hexavalent chromium removal. *Environmental Research*, 187, p.109694. https://doi.org/10.1016/j.envres.2020.109694.

Rath, J., Sahoo, J.K., Sukla, R.K., Pradhan, A., Biswal, S.K., Dwivedy, P. and Sahoo, S.K., 2024. Eriochrome Black T dye removal from an aqueous solution using graphene oxide-modified activated carbon materials. *Indian Chemical Engineer*, pp.1–20. https://doi.org/10.1080/00194506.2024.2342845.

Reck, I.M., Paixão, R.M., Bergamasco, R., Vieira, M.F. and Vieira, A.M.S., 2018. Removal of tartrazine from aqueous solutions using adsorbents based on activated carbon and *Moringa oleifera* seeds. *Journal of Cleaner Production*, 171, pp.85–97. https://doi.org/10.1016/J.JCLEPRO.2017.09.237.

Ren, B., Jin, Y., zhao, L., Cui, C. and Song, X., 2022. Enhanced Cr(VI) adsorption using chemically modified dormant *Aspergillus niger* spores: Process and mechanisms. *Journal of Environmental Chemical Engineering*, 10(1), p.106955. https://doi.org/10.1016/j.jece.2021.106955.

Sadeghi, S., Zakeri, H.R., Saghi, M.H., Ghadiri, S.K., Talebi, S.S., Shams, M. and Dotto, G.L., 2021. Modified wheat straw–derived graphene for the removal of Eriochrome Black T: characterization, isotherm, and kinetic studies. *Environmental Science and Pollution Research*, 28(3), pp.3556–3565. https://doi.org/10.1007/s11356-020-10647-w.

Salomón, Y.L.D.O., Georgin, J., Franco, D.S.P., Netto, M.S., Piccilli, D.G.A., Foletto, E.L., Oliveira, L.F.S. and Dotto, G.L., 2021. High-performance removal of 2,4-dichlorophenoxyacetic acid herbicide in water using activated carbon derived from Queen palm fruit endocarp (*Syagrus romanzoffiana*). *Journal of Environmental Chemical Engineering*, 9(1), p.104911. https://doi.org/10.1016/j.jece.2020.104911.

Sandhu, K.S. and Lim, S.T., 2008. Structural characteristics and in vitro digestibility of Mango kernel starches (*Mangifera indica L.*). *Food Chemistry*, 107(1), pp.92–97. https://doi.org/10.1016/J.FOODCHEM.2007.07.046.

dos Santos, C.C., Mouta, R., Junior, M.C.C., Santana, S.A.A., Silva, H.A. dos S. and Bezerra, C.W.B., 2018. Chitosan-edible oil based materials as upgraded adsorbents for textile dyes. *Carbohydrate Polymers*, 180, pp.182–191. https://doi.org/10.1016/J.CARBPOL.2017.09.076.

Sing, K.S.W., Everett, D.H., Haul, R.A.W., Moscou, L., Pierotti, R.A., Rouquerol, J. and Siemieniewska, T., 1985. Reporting Physisorption Data for Gas/Solid Systems with Special Reference to the Determination of Surface Area and Porosity. *Pure and Applied Chemistry*, 57(4), pp.603–619. https://doi.org/10.1351/PAC198557040603/MACHINEREADABLECITATION/RIS.

Thommes, M., Kaneko, K., Neimark, A. v., Olivier, J.P., Rodriguez-Reinoso, F., Rouquerol, J. and Sing, K.S.W., 2015. Physisorption of gases, with special reference to the evaluation of surface area and pore size distribution (IUPAC Technical Report). *Pure and Applied Chemistry*, 87(9–10), pp.1051–1069. https://doi.org/10.1515/PAC-2014-1117/PDF.

Tonato, D., Drumm, F.C., Grassi, P., Georgin, J., Gerhardt, A.E., Dotto, G.L. and Mazutti, M.A., 2019. Residual biomass of Nigrospora sp. from process of the microbial oil extraction for the biosorption of procion red H–E7B dye. *Journal of Water Process Engineering*, 31, p.100818. https://doi.org/10.1016/j.jwpe.2019.100818.

Treviño-Cordero, H., Juárez-Aguilar, L.G., Mendoza-Castillo, D.I., Hernández-Montoya, V., Bonilla-Petriciolet, A. and Montes-Morán, M.A., 2013. Synthesis and adsorption properties of activated carbons from biomass of *Prunus domestica* and *Jacaranda mimosifolia* for the removal of heavy metals and dyes from water. *Industrial Crops and Products*, 42(1), pp.315–323. https://doi.org/10.1016/J.INDCROP.2012.05.029.

Wei, Y., Salih, K.A.M., Rabie, K., Elwakeel, K.Z., Zayed, Y.E., Hamza, M.F. and Guibal, E., 2021. Development of phosphoryl-functionalized algal-PEI beads for the sorption of Nd(III) and Mo(VI) from aqueous solutions – Application for rare earth recovery from acid leachates. *Chemical Engineering Journal*, 412, p.127399. https://doi.org/10.1016/J.CEJ.2020.127399.

Yao, T., Qiao, L. and Du, K., 2020. High tough and highly porous graphene/carbon nanotubes hybrid beads enhanced by carbonized polyacrylonitrile for efficient dyes adsorption. *Microporous and Mesoporous Materials*, 292, p.109716. https://doi.org/10.1016/J.MICROMESO.2019.109716.

Yin, K., Wang, Q., Lv, M. and Chen, L., 2019. Microorganism remediation strategies towards heavy metals. *Chemical Engineering Journal*, 360, pp.1553–1563. https://doi.org/10.1016/J.CEJ.2018.10.226.